DOI: 10.1002/ smll.201902058R1

Article type: Full Paper

Title:

Rapid production of cell-laden microspheres using a flexible microfluidic encapsulation platform

Author(s), and Corresponding Author(s): Wen J. Seeto, Yuan Tian, Shantanu Pradhan, Petra Kerscher, Elizabeth A. Lipke**

Dr. W. J. Seeto, Y. Tian, Dr. S. Pradhan, Dr. P. Kerscher, Prof. E. A. Lipke

The first 2 authors contributed equally to the manuscript

212 Ross Hall, Auburn, AL 36849, USA
E-mail: eal0003@auburn.edu

Keywords: hydrogel microspheres, microfluidic encapsulation, photocrosslink, biomanufacturing, regenerative medicine

Abstract:

This study establishes a novel microfluidic platform for rapid encapsulation of cells at high densities in photocrosslinkable microspherical hydrogels including poly(ethylene glycol)-diacrylate (PEGDA), poly(ethylene glycol)-fibrinogen (PF), and gelatin methacrylate (GelMA), enabled by a new molding technique for microfluidic device fabrication. Cell-laden hydrogel microspheres are advantageous for many applications from high-throughput drug screening to regenerative medicine. Employing microfluidic systems is considered the most efficient method for scale-up production of uniform microspheres. However, existing platforms have been constrained by traditional microfabrication techniques for microfluidic device fabrication, restricting microsphere diameter to below 200 µm and making iterative design changes time-consuming and costly. Using the new molding technique, the microfluidic device employs a modified T-junction design with readily adjustable channel sizes, enabling production of highly uniform microspheres with high cell densities (10-60 million cells mL^{-1}) and a wide range of diameters (300-1100 µm), which are critical for realizing downstream applications,

through rapid photocrosslinking (≈1s per microsphere). Multiple cell types are encapsulated, are evenly distributed throughout the microspheres, and maintain high viability and appropriate cellular activities in long-term culture. This microfluidic encapsulation platform is a valuable and readily adoptable tool for numerous applications, including supporting injectable cell therapy, bioreactor-based cell expansion and differentiation, and high throughput tissue sphere-based drug testing assays.

1. Introduction

Hydrogel microspheres are advantageous for use in a wide range of regenerative medicine applications,[1] including 3D cell culture,[2] injectable cell delivery,[3] disease modeling,[4] cell differentiation,[5] drug delivery,[6] vaccine production,[7] and cell production.[8] Depending on the application, cells can be either encapsulated within or seeded on the surface of the microspheres, in which case they are referred to as microcarriers.

Microspheres can be fabricated using extrusion, atomization, emulsion, and microfluidics. Among these methods, emulsion and microfluidics are used more widely because they do not require the specialized equipment necessary for the other methods.[9] Although emulsion allows for scalable production and has been used successfully for mammalian cell encapsulation,[10-11] this method of microsphere production has some inherent challenges. The emulsion process can require the use of harsh chemical solvents, necessitating further processing steps to minimize the negative impact on downstream cell viability, and can be time-consuming depending on the crosslinking method.[12-13] Incorporating cells directly is also challenging; the high levels of shear stress make consistent maintenance of high cell viability during the emulsion process difficult. In addition, microspheres produced from emulsion usually have a broad size distribution which can be problematic for downstream applications where tight size distribution is critical.[14] In contrast, microfluidic approaches can precisely produce uniform microspheres with a very narrow size distribution (coefficient of variance, CV < 5%).[15] However, due to constraints in channel dimensions imposed by the use of photolithography for microfluidic chip fabrication, resulting microspheres typically have a maximum diameter of around 200 μm.[16] Furthermore, pressure differences and changes in flow stability within these smaller channels make it more challenging to encapsulate cells at high densities or in cell clusters, which tend to clog the microfluidic channels and junctions.[15] High cell density is critical for therapeutic cell delivery as we have shown in previous work, where millions of cells were used for large animal cell therapy.[17] To minimize the delivered volume and fabrication time while achieving the desired therapeutic dose, high cell densities were required. However, the small dimensions of microfluidic chips limit the total number of cells that can be encapsulated per time, failing to meet the needs for therapeutic cell delivery. Additionally, there are other restrictions on the applications of microspheres where larger size microspheres are desired, for example, modeling large tumors for induction of hypoxia and necrosis, providing shear-protection for bioreactor-based cell production, and improving retention of injected therapeutic cells. In addition to the limitation on channel size, the complex process of photolithography makes adjustment of the channel dimensions of microfluidic chip difficult. It requires a substantial

investment of time and resources to produce a microfluidic chip with a different design during process optimization.

Having reported the use of hydrogel microspheres for large animal cell therapy,[17] here we present for the first time the design of the custom-built microfluidic platform that overcomes some of the challenges inherent to microfluidic cell encapsulation using standard microfluidic chips. The microfluidic device, which is the major component of the platform, leverages the use of 3D printing for scalable mold production and a custom-developed molding technique that does not require expensive reagents and facilities for photolithography. With a custom-designed T-junction and readily adjustable assembling components, the platform enables rapid production of microspheres with a wide range of diameters from 300 µm to 1100 µm. This robust platform also has the potential to be used with a variety of natural and synthetic polymers; here we have demonstrated microspheres produced with poly(ethylene glycol) diacrylate (PEGDA), poly(ethylene glycol)-fibrinogen (PF), and gelatin methacrylate (GelMA) through rapid photocrosslinking. With the use of Eosin Y as the photoinitiator and a full spectrum light source, cells at high density (10-60 million cells mL^{-1} of hydrogel precursor solution, depending on application) were encapsulated including horse endothelial colony forming cells (ECFCs), breast cancer cells, or human induced pluripotent stem cells (hiPSCs). The encapsulated cells were evenly distributed through the microspheres and maintained high viability and functional cellular activities. These results demonstrate the capabilities of this microfluidic encapsulation platform and show its potential for various regenerative medicine applications.

2. Results and Discussion

This study established a novel microfluidic encapsulation platform and developed a new method for microfluidic device fabrication to overcome the limitations imposed by photolithography. Deviating from traditional microfluidic chip fabrication, this study established a novel molding technique for fabricating microfluidic devices. The resulting devices employ a custom-designed T-junction and continue to provide the important advantages of using microfluidic systems for production of hydrogel microspheres. This new molding technique supports designing microfluidic devices with a wider range of dimensions for various components, including junction geometry, channel width, and device length. The ease and flexibility provided by this technique enables quick fabrication of prototypes for ready testing and design iteration, which is beneficial for understanding the fluid dynamics of microsphere production. The established microfluidic encapsulation platform was shown to be compatible with multiple polymers and cell types, and was able to produce highly uniform microspheres with high cell densities and a wide range of diameters through rapid photocrosslinking. The encapsulated cells were evenly distributed through the microspheres and could maintain high viability and cellular activities in long-term culture post-encapsulation.

2.1. Microfluidic encapsulation platform using a novel custom design and device molding technique

A novel microfluidic encapsulation platform was developed in this study. As shown in **Figure 1**A-B, the microfluidic encapsulation platform is composed of three syringe pumps, a collection vessel, and the novel custom-designed polydimethylsiloxane (PDMS) microfluidic device. Aqueous polymer precursor solution, the discrete phase, flows into the device through the top inlet channel and the oil, the continuous phase, flows in through the bottom channel. The flow rate of the polymer precursor and oil can be independently adjusted using two syringe pumps, providing control over the polymer precursor/oil flow rate ratio. Microspheres are formed at the T-junction due to emulsification and then photocrosslinked in the outlet channel of the microfluidic device (Video S1, Supporting Information), using a wide spectrum visible light source with a liquid light guide. At the end of the outlet, the microsphere hydrogels are washed down with and collected in media, controlled by a syringe pump.

This encapsulation platform uses a high power visible light source to perform rapid photocrosslinking, which leads to a much higher production rate. Compared to other microfluidic platforms, microspheres here have a much shorter residence time passing through the light beam. It takes approximately 1 s for photocrosslinking, whereas other platforms take up to 20 s or longer per microsphere.[18-19] As previously reported, using this platform 4 million cells were encapsulated in 400 µL of PF precursor solution in 24 minutes, resulting in approximately 1500 cell-laden microspheres with diameters of 800 µm.[17] A range of power output (0.5 W- >3 W, 10%-100%) of the light source has been tested. In order to achieve rapid photocrosslinking, a minimum of 2.8 W cm^{-2} light was necessary to form microspheres with stable boundaries and structural integrity, and a mirror was placed behind the device to reflect the light for higher crosslinking efficiency. Power output can be increased for photocrosslinking without affecting the microsphere size and geometry. In addition to the light source power output, many other platform parameters were established through extensive iterative testing. For example, the distance of the light source from the outlet channel was optimized to support rapid photocrosslinking while keeping heat generation low enough to maintain high cell viability. Further improvements could be achieved by the use of an LED light source.

As the major component of the platform, the microfluidic devices are fabricated using a new molding technique that is more flexible than the standard microfabrication techniques employed for microfluidic chip production. When using standard photolithography microfabrication techniques, the maximum diameter of fabricated microspheres is generally determined by the height of microfluidic channels, which is usually around 200 µm.[16] This limitation is a result of the channel height being dictated by the maximum thickness of photoresist that can be cast onto a wafer and depends on the series and choice of the photoresist. As a result, traditional microfluidic device fabrication is not suitable when microspheres with larger diameters are desired. This study overcomes the size limitation by employing a molding technique and designing a suitable T-junction in the fabrication of the microfluidic device.

The design of the microfluidic device channels is assembled with easily acquired components as shown in the Experimental Section. Numerous iterations were able to be performed in the design of the reported device due to the ease of fabrication using the molding technique. In order to hold the assembly of the channels together and control the dimension of the microfluidic device, a reusable channel mold-holding jig was designed (**Figure S1**, Supporting Information) and 3D printed (Figure 1C) with acrylonitrile butadiene styrene (ABS) filament (The 3D printable file of the jig is available upon request). The 3D printed jig is essential for consistent and scalable production of microfluidic devices. In addition, the cost of all components is relatively low (Figure 1D, detailed cost shown in Experimental Section). After the PDMS is cured, the molds of the channels can be easily removed (Figure 1E). Producing a microfluidic device with new channel dimensions takes approximately 1 hour, which allows for quick testing during prototype development. Although this molding fabrication approach may not provide the high level of consistency needed to commercially manufacture numerous identical microfluidic devices, it eliminates the need to use photolithography, making it advantageous for research groups wanting to do rapid, iterative design testing or for those who do not have ready access to expensive microfabrication facilities.

Based on iterative testing, the final design of the microfluidic device is shown in Figure 1F. The T-junction and the channels are molded with Teflon tubes and metal wires, providing channels with a circular cross-sectional area instead of the rectangular cross-sectional area produced using photolithography. In typical T-junction designs, the two inlet channels are perpendicular to each other, with the discrete phase entering the continuous phase channel at an angle and then progressing linearly to the outlet.[20-21] Here, however, the discrete and continuous phase inlet channels are collinear with each other and the joint outlet channel is perpendicular to both inlets. When the microfluidic device is placed vertically, the collinear inlet channels can maximally exploit the density difference between two fluids to assist droplet formation, which will be discussed in the following paragraph. This unique design leverages the simplicity of the T-junction design while providing additional control over microsphere size and operational stability, typically only achieved using much more complex flow focusing microfluidic designs. In particular, manipulation of the inlet flow ratio enables control over microsphere size. This T-junction design has not to our knowledge been used before for microsphere fabrication. The top inlet channel was designed to contain a restriction segment as indicated by an asterisk. This was implemented to stabilize the precursor/oil interface prior to entering the outlet channel; without this restriction segment some of the denser precursor tends to escape from the aqueous flow into the oil phase and form unwanted droplets that sink to the bottom inlet in the vertically oriented device. Beneath the restriction segment is a conical region instead of a cylindrical region, which was introduced to eliminate the dead volume of hydrogel precursor solution. The metal wire has a tapered end that can be inserted into the Teflon tube forming the T-junction. The tapered end slightly increases the flow speed at the T-junction to aid in microsphere formation. This approach is commonly used in microfluidic flow focusing techniques [22-23] but not in standard T-junctions, where only the discrete stream (aqueous/polymer precursor) is entering the continuous stream at an angle, versus our modified T-junction design where both the continuous and discrete streams are perpendicular to the outlet channel. The metal wires have different sizes and can be easily machined to obtain desired tapered end, providing

flexibility in adjusting channel size and junction geometry. Since rapid photocrosslinking requires a high-power light source, the outlet channel length in this design was increased to achieve an optimal distance between the T-junction and the light source to minimize the influence of light back scattering. Previously, multiple methods were reported to prevent scattered light from reaching the junction, including embedding opaque materials in the device and reducing light power which resulted in extended crosslinking time.[24] External shielding methods combined with opaque material embedding were tested in earlier iterations of the reported platform. However, it was determined that light was traveling down the interior of the outlet channel itself. As readily facilitated by the employed molding technique, the device length was extended to 10 cm, which provided the distance between the light source and the T-junction needed to eliminate this issue.

The microfluidic device orientation within this platform is also a critical design parameter. In contrast to typical microfluidic device operation, the one in this study is orientated vertically instead of lying flat horizontally.[25] Since the channel sizes are much larger than in traditional microfluidic chips, gravity is an important factor in successful device operation and needs to be considered. According to our preliminary studies during platform development, the vertical orientation allows the less dense oil, which is flowing in from the bottom inlet, to separate the denser hydrogel precursor/cell-precursor suspension, which is flowing in from the top inlet, in a more stable manner. Combining all the new design features mentioned above, the resulting microfluidic encapsulation system is able to rapidly produce uniform microspheres with a wide range of diameters from 300 µm to 1100 µm (Figure 1G-J) that can be used for numerous applications, including injectable cell delivery, bioreactor-based cell expansion and differentiation, and tissue sphere-based drug testing assays.

In addition to the design of the microfluidic device itself, the collection wash fluid that flows over the outlet port at the end of the device is also critical to flow stabilization. Exiting microspheres are washed down from the end of the outlet channel into the collection tube resulting in them being immediately immersed in cell culture media. Without this wash stream, accumulation of microspheres at the outlet introduces unstable flow within the upstream channels which results in wide distribution of microsphere diameter and geometry. This is a novel approach that to our knowledge has not been employed in other systems. Furthermore, such stable system flow enables the formation of a range of microsphere diameters within a range of flow rates by using a single microfluidic device design. More details will be discussed in a later section. Taken together with the novel custom-designed microfluidic device made by molding, this encapsulation platform can overcome the limitations of traditional microfluidic chip-based production and produce uniform microspheres with a wide range of diameters.

2.2. Established microfluidic encapsulation platform is compatible with multiple photocrosslinkable polymers

Using the established microfluidic encapsulation platform, microspheres have been produced using multiple photocrosslinkable polymers that have been widely employed for various tissue engineering applications.[26-27] Here, we examined the photocrosslinkable hydrogel materials PF, GelMA, and PEGDA; these materials have been used for cancer tissue engineering,[11] cardiac tissue engineering,[28-29] and bone regeneration.[30] These polymers were selected to demonstrate the compatibility of this setup with various polymers. The presence of the acrylate groups allows crosslinking and formation of hydrogels through free-radical chemistry.[31] The photoinitiator in polymer precursor solution triggers the photocrosslinking reaction once exposed to light. Acellular microspheres were fabricated with each of these polymers; scanning electron microscopy (SEM) images of the microspheres showed the typical porous structure present in these hydrogel scaffolds (**Figure 2**A-D).[32] Using the same parameters for microsphere production, elastic moduli of microspheres formed using the three different polymers were evaluated by a compression testing (Figure 2E and F). All microspheres were observed to regain their initial geometries following compression (Video S2, Supporting Information). Elastic moduli of PF, GelMA, and PEGDA were found to be 127.3 ± 24.4 Pa, 1894 ± 257 Pa, and 31,800 ± 5,280 Pa respectively (Figure 2G). Collectively, these results demonstrate that this microfluidic encapsulation platform has the capability to be used for producing microspheres with various polymer systems.

2.3. Straightforward control of microsphere diameters by varying inlet flowrates and outlet channel diameter.

In addition to fabricating microspheres with various materials, this microfluidic device also provides tight control over microsphere diameter. Based on extensive testing during platform development using multiple microfluidic device designs, the ratio of precursor to oil flow rate and outlet channel diameter were found to be the critical parameters in controlling microsphere diameter. For example, by changing the precursor: oil flow rate ratio from 1:10 to 2:9 in a microfluidic device with 750 µm outlet channel diameter, the microsphere diameter increased from 746 ± 46 µm to 788 ± 40 µm (**Figure 3**A). Similarly, microspheres increased in diameter from 811 ± 22 µm to 951 ± 25 µm when changing the precursor: oil flow rate ratio from 1:10 to 2:9 in the microfluidic device with 920 µm outlet channel diameter (Figure 3A). These results demonstrate the diameters of microspheres can be changed by varying just the precursor: oil flow rate ratio without changing the outlet channel diameter. Conversely, when holding the flow rate ratio constant, the resulting microspheres were bigger in size as the outlet channel diameter was increased (Figure 3A). Roundness was found to be above 0.95 for all microspheres (Figure 3B). Representative images are shown in Figure 3C-F.

In flow focusing and co-flow microfluidic chips, varying the inlet flow rate ratio is a common approach to adjust the size of the microspheres, and both experimental[33] and computational[34] studies have been done. Channel diameter is the limiting factor in determining the maximum size of produced microspheres. Because of the constraints imposed by photolithography, traditional microfluidic chip fabrication is time-consuming and has an upper limit of 200 µm for channel

diameter.[35] By employing the molding technique used here in microfluidic device fabrication, the outlet channel diameter can be altered simply by selecting a different wire size for molding. The metal wire used in molding the outlet channel is commercially available in a wide range of diameters (250 µm – 25 mm). This is highly advantageous for maximizing the microsphere diameter options available for specific applications, providing much greater flexibility than microfabrication. Together these results show that microsphere diameter can be readily controlled by adjusting inlet flowrates and altering outlet channel diameter.

2.4. Highly uniform microspheres produced within and between batches

Tight control over the size and shape of microspheres is critical for various applications, such as high-throughput drug screening,[36] cell production,[37] bioprinting using microspheres as building blocks,[38] and cell delivery.[17] For regenerative medicine, high uniformity of microspheres prepared from multiple batches is needed to ensure smooth and consistent cell delivery by injection. For high-throughput drug screening, tight control over size and shape of microspheres enables a better comparison of drug effects and reduces the number of required replicates. The microfluidic encapsulation platform presented in this study provides high uniformity of produced microspheres both between and within batches. As shown in **Figure 4**A-C, horse ECFCs were encapsulated within PF hydrogel microspheres at the high cell densities required for therapeutic cell delivery; these ECFC-laden microspheres, which are shown in fluorescent green, were highly consistent. Five separately prepared batches of ECFCs-laden microspheres were analyzed quantitatively for intra- and inter-batch comparison (Figure 4D); average microsphere diameter ranged from 740 µm to 793 µm between batches with low variance (CV < 2%) within each batch. For each of the five batches, average roundness was above 0.980 with a standard deviation of 0.01 between microspheres.

Moreover, cell distribution within the microspheres was also assessed. Horse ECFC microspheres were cryosectioned after encapsulation. Cells were found to be distributed evenly throughout the microsphere volume as shown in Figure 4E. Collectively, these results show that the microspheres produced by this microfluidic encapsulation platform have highly uniform size, shape, and inner cell distribution.

2.5. Established microfluidic platform enables encapsulation with high cell density

Encapsulation of cells at high densities and/or in clusters, rather than as single cells, creates substantial additional technical challenges, particularly in maintaining microsphere uniformity. Most studies on microfluidic encapsulation have reported producing microspheres with low cell densities,[39-40] and very few studies have been conducted using higher cell densities (1-10 million cells mL^{-1}).[41] This limitation is due to the junction becoming clogged and/or changes in the precursor viscosity. However, producing microspheres with a high cell density is critical for many downstream applications, including delivery of sufficient numbers of cells to achieve therapeutic benefit without exceeding limitations on injection volume.

Encapsulation at high cell density for both single cells and cell clusters was tested. Following the design modifications described above for enhanced operational stability, the microfluidic device operated robustly under these challenging conditions. Single cells including horse ECFCs and MCF7

cells, and clusters of hiPSC were encapsulated at 10 million cells mL^{-1}, 20 million cells mL^{-1}, and 25 million cells mL^{-1}, respectively (**Table 1**). The hiPSC clusters did not clog the junction. Resulting microspheres were uniform in size and shape for all encapsulation densities and had similar diameters post-encapsulation as shown in **Figure 5**A-C. Diameters of hiPSC, horse ECFC, and MCF7 microspheres were 878 ± 29 µm, 957 ± 31 µm, and 939 ± 26 µm (n>20 microspheres for each cell type), which all show low standard deviation. High degree of roundness (above 0.95) was maintained for all cell types (Figure 5D). Furthermore, MCF7 cells at 60 million cells mL^{-1} could be encapsulated without clogging the microfluidic device and the resulting microspheres were highly uniform with diameters of 979± 13 µm and roundness of 0.98± 0.01 (Table 1).

Cell viability was evaluated post-encapsulation in all design iterations to assess the effect of device-associated shear stress and light exposure on the cells during encapsulation with this platform. Horse ECFCs, MCF7 cells, and MDA-MB-231 cells were found to have a high post-encapsulation viability of 97 ± 1%, 98 ± 1%, and 97 ± 1%, respectively. Microsphere encapsulated hiPSC clusters were also found to have high viability (Figure 5E). Accurate quantification without further processing to dissociate the cell clusters, which inherently reduces viability, was not possible. Results indicate that the microfluidic platform enables encapsulation at high cell densities while maintaining high cell viability. These results advance the ability to achieve commercial applications of cell-laden microspheres, such as therapeutic cell delivery, stem cell differentiation, and cancer tissue modeling.

2.6. Cells maintain normal cellular activities post encapsulation

Following encapsulation in the microfluidic platform, understanding the potential impact of this process on subsequent cellular function is important for downstream applications. Cells were found to maintain normal cellular activities after being encapsulated, including the ability to proliferate within the microspheres and to remodel the microsphere structure. As a proof-of-concept, horse ECFCs were encapsulated in PF hydrogel microspheres and their cellular activities were assessed, including cell outgrowth, alteration of microsphere stiffness and morphology, and cell proliferation marker expression. When culturing the ECFC-laden microspheres in collagen-coated well plates, ECFCs had round morphology upon encapsulation. Then the cells were seen to elongate and align along the edges of the hydrogel microspheres one day after encapsulation (**Figure 6**A). Generally, changes in cell morphology can be caused by external force exerted on cells from different sources, such as magnetic forces,[42] shear stress,[43] or interaction between cell adhesion molecules and their ligands.[44] Here, ECFC morphology changed through cellular binding to cell-adhesion sites provided by the fibrinogen in the PF hydrogel as shown in **Figure S3**A (Supporting Information).

On day 3, cell outgrowth from the microsphere was observed, and these cells formed a confluent layer (Figure 6B). The elastic modulus of the ECFC-laden microspheres was measured and found to increase significantly from day 1 to day 3 (Figure 6C), indicating the encapsulated cells were actively remodeling the microspheres. In-depth analysis for all cell types, although beyond the scope of this study, is ongoing for horse ECFCs,[17] breast cancer cells, and hiPSCs. Cellular activity of encapsulated cells was found to differ between cell types, as expected based on the phenotypic differences. For example, rate of remodeling and changes in elastic modulus have been observed to

be cell type dependent (results shown in Figure S2C, Supporting Information). Additionally, size and shape of the ECFC-laden microspheres from 3 batches were quantified on day 0, 1, and 3 (Figure 6D-E). Both the diameter and roundness of the microspheres decreased along with time as a result of cellular activities of the encapsulated cells. Encapsulation did not substantially impact cell proliferation; the vast majority of ECFCs continued to show positive Ki67 expression on both day 0 and day 4 post-encapsulation as shown in Figure 6F-G. Multiple batches of ECFC microspheres were maintained in culture for over one month; similar cellular growth and PF microsphere remodeling was observed over time as shown in Figure S3B (Supporting Information). Taken together, these results provide initial evidence that the cells maintain viability and basic cellular activities following encapsulation using the microfluidic platform and justify further in-depth application-specific studies.

2.7. Resulting microspheres enable long term cell culture

Encapsulated cells can be cultured long-term within the microspheres. To demonstrate this, MCF7 breast cancer cells and MDA-MB-231 breast cancer cells were separately encapsulated in PF hydrogel microspheres (20 million cells mL^{-1}) and cultured for at least one month. MCF7 cells grew as distinct local colonies with tight cell packing, as is characteristic of this cell type in 3D culture, and colonies were distributed uniformly throughout the microsphere. Colony outgrowth of MCF7 cells was observed under phase contrast microscope from day 14 to day 28 after encapsulation as shown in **Figure 7**A-C. In SEM images of the microspheres, increasing outgrowth of MCF7 cell colonies from the hydrogel material was seen over time (Figure 7E-H). Encapsulated MDA-MB-231 cells were cultured for over 38 days, with continued maintenance of cell viability (Figure 7D). Multiple cell types have been tested and were able to maintain viable for an extended period of time. Comprehensive studies of long-term culture are in progress for breast cancer cells, horse ECFCs,[17] and hiPSCs. Together, these results suggest that microspheres produced using the microfluidic encapsulation platform can be used for long term cell culture.

To meet the need for a wide range of downstream applications, the field of tissue engineering needs to be able to rapidly encapsulate mammalian cells at high cell density in uniform microspheres using clinically applicable materials with tight control over microsphere shape and size, while maintaining high cell viability and cellular phenotype. However, the commercially available systems for cell-laden hydrogel microspheres production are mainly based on electrostatically assisted spraying (or electrospray) technology. Produced cell-laden droplets are polymerized through exposure to ions in the collection solution. Limited by this polymerization approach, encapsulation systems using electrospray are limited to use with only a few types of materials, such as alginate and agarose-based materials, and polymerization time can be up to 5-10 minutes. Given the tighter control over microsphere size and more flexibility in terms of crosslinking approach and material selection, microfluidic systems have the potential to bridge the technological gap for realizing downstream commercial applications and have a competitive advantage in the marketplace. However, most microfluidic systems on the market and reported previously in the scientific literature only work with acellular materials or very low cell densities, and the resulting microspheres are small in size, which is limited by microfabrication technique used during

microfluidic device production. Here we have described multiple advantageous features that can be employed to advance microfluidic platforms towards commercially applicable production, including rapid production rate, wide range of sizes, materials selections, cell densities, and cell types, and easy device fabrication method, making the platform to be adopted by others easily. A table comparing current encapsulation systems and the novel microfluidic platform we developed is shown in **Table 2**, and more detailed information is shown in **Table S1-3** (Supporting Information).

3. Conclusion

This study established a robust microfluidic cell encapsulation platform, including developing a new molding technique for microfluidic device fabrication (**Figure 8**). This new method overcomes the limitations imposed by traditional microfluidic chip fabrication using photolithography and provides great flexibility for altering the design of the microfluidic device. With a custom-designed T-junction and readily adjustable channel sizes, the established microfluidic encapsulation platform is compatible with multiple polymers and cell types; furthermore it can be used to produce highly uniform microspheres with high cell densities and a wide range of diameters through rapid photocrosslinking. The encapsulated cells are evenly distributed through the microspheres and can maintain high viability and appropriate cellular activities in long-term culture. This microfluidic encapsulation platform can be a valuable tool for tissue engineered microsphere production for use in regenerative medicine applications. More studies for a thorough understanding of the fluid dynamics during microsphere production will be carried out in the future.

4. Experimental Section

Cell culture: Isolation and culture of horse endothelial colony forming cells (ECFCs) from horse peripheral blood were performed based on a method that was previously published.[51] All procedures involving animals were approved by the Auburn University Animal Care and Use Committee. ECFCs were cultured in Endothelial Cell Basal Medium-2 (Lonza) containing 5% horse serum (HyClone) and SingleQuots Kit (Lonza) at 37°C and 5% CO_2. The ECFCs were seeded and expanded on collagen-coated tissue culture polystyrene flask. When ECFCs reached 90% confluency, trypsin/EDTA (Lonza) was added to detach the cells at 37°C for 50 s and was neutralized by ECFCs medium followed by centrifugation at 200 g for 5 min. ECFCs were resuspended in medium and then subcultured at a ratio of 1:6 or immediately used for experiment. Cells between passage 2-7 were used for all experiments.

MCF7 (ATCC®HTB-22™) and MDA-MB-231 (ATCC®HTB-26™) human breast cancer cells were maintained in Dulbecco's Modified Eagle's Medium (DMEM, Gibco) supplemented with 10% fetal bovine serum (FBS, Atlanta Biologicals), 1% (v/v) non-essential amino acids (Lonza), 1% (v/v)

penicillin/streptomycin, 1% (v/v) Glutamax (Gibco), and 1% (v/v) sodium pyruvate. Cells were expanded and dissociated with trypsin/EDTA when reaching 90% confluency.

IMR-90 Clone 1 and 19-9-11 (WiCell) human induced pluripotent stem cells (hiPSCs) were cultured on human embryonic stem cell (hESC) qualified Matrigel (Corning) using mTeSR-1 medium (Stem Cell Technologies) and passaged using Versene (Invitrogen).

PEGDA synthesis: Poly(ethylene glycol) (PEG, 10kDa; Sigma) was acrylated to form PEG-diacrylate(PEGDA) following a method from a previously published literature.[52] Briefly, PEG was first lyophilized, and then reacted with 0.4 M acryloyl chloride (Alfa Aesar) and 0.2 M triethyl amine (TEA, Sigma) in anhydrous dichloromethane (Acros) under argon overnight. 1.5 M K_2CO_3 (Fisher) was then added, and the solution was separated into aqueous and organic phase. The organic phase was collected and dried with anhydrous $MgSO_4$ (Fisher). The PEGDA was then precipitated by cold ethyl ether, filtered, dried, and stored under argon at -20°C. The degree of acrylation was estimated to be 96.0% by NMR. PEGDA was dissolved in phosphate-buffered saline (PBS, Lonza) to 10% (w/v) prior to use.

PEG-fibrinogen synthesis: PEG-fibrinogen (PF) was synthesized by following a previously published method.[53] In brief, fibrinogen (Type I-S; Sigma) was dissolved in 8 M urea (Sigma) in PBS (Lonza) solution to a final concentration of 7 mg mL^{-1} with pH of 7.4. Then tris(2-carboxyethyl) phosphine (Acros Organics) was added to the solution and reacted at pH of 8. PEGDA was dissolved in urea-PBS to a final concentration of 280 mg mL^{-1} and then slowly added to fibrinogen solution to react for 3 hours in dark at room temperature. After reaction, PEGylated fibrinogen was precipitated with acetone, followed by centrifugation to remove acetone, and then dissolved in urea-PBS again for dialysis. The product was dialyzed in sterile PBS over 24 hours in dark at 4°C, and then stored at -80°C. Protein content was calculated to be 12.5 mg mL^{-1} using a Pierce BCA protein assay kit (Thermo Fisher). PEGylation yield was calculated to be 98.1%.

GelMA synthesis: Methacrylated gelatin (GelMA) was synthesized following previous protocols[54-55] with modifications. Briefly, gelatin (Type B, bovine) was mixed at 5% (w/v) into phosphate buffered solution (PBS, Gibco) at 60 °C with constant stirring until fully dissolved. Methacrylic anhydride (MA) was slowly added until the target concentration was reached (15% w/v) and reacted at 60 °C for 2 h. The reaction was stopped with PBS; methacrylated gelatin was dialyzed for seven days and lyophilized for five days. Lyophilized GelMA was dissolved in deuterium oxide (Fisher Scientific) for NMR analysis. ^{1}HNMR spectra were collected using a Bruker NMR spectrometer. Before integration, phase and baseline corrections were applied to ensure accurate methacrylation calculations. GelMA was dissolved in PBS to 1.5% (w/v) and kept at 37ºC prior to use.

3D printed bracket for scale up production of microfluidic device: A bracket was 3D printed to hold the mold for creating the junction and the channels for the microfluidic device. The bracket was designed in Blender 2.77 and printed using the LulzBot TAZ 5 with an acrylonitrile butadiene styrene (ABS) filament. The T-junction and the channels were molded with Teflon tubes and metal wires. To assemble the mold, two hollow Teflon tubes were inserted into the holes on the jig as shown in Figure S1 and Figure 1D. The top Teflon tube had a cylindrical end and the bottom one had a conical end for making the conical region at the junction. A metal wire was inserted into the hollow center of both Teflon tubes, and the uncovered part of the wire in between tubes could form a restriction segment. Another metal wire with tapered end was introduced through the third hole on the jig and inserted right below the conical end of the Teflon tube to make the outlet channel. The metal wires have different sizes and can be easily machined to obtain desired tapered end, providing flexibility in adjusting channel size and junction geometry. Multiple design parameters of assembled junction, including junction size, tapered end length, and outlet channel size were then checked under microscope to ensure consistency in device fabrication.

After the channels were assembled to achieve the desired junction design, the bracket was fixed on a glass using binder clips. Polydimethylsiloxane (PDMS) microfluidic device was created with Sylgard 184 silicone elastomer kit (Dow Corning) by pouring the mixture of base and cure component into the bracket, and air bubbles were removed by vacuum. Then the PDMS was cured at 70°C for 2 hours. Once the PDMS was cured, the channel molds were removed and the PDMS was extracted from the bracket. The PDMS was cleaned by sonicating in 70% ethanol before and after each use. The total cost of each microfluidic device was estimated to be $2.90, which included the cost of all components of the channels ($0.80 per device), the jig ($0.16 per device), and PDMS (14 g, $1.94 per device).

Cell encapsulation in hydrogel microspheres: Cell encapsulation in hydrogel microspheres was achieved through the novel microfluidic encapsulation platform. Before cell encapsulation, hydrogel precursor solution was prepared by mixing the polymer solution (PEGDA, PF, or GelMA) with 0.1% (w/v) of Pluronic F68 (Sigma), 0.1 mM of Eosin Y photoinitiator (Fisher Scientific), 1.5% (v/v) triethanolamine (Acros Organics), and 0.39% (v/v) of N-vinylpyrrolidone (Sigma). Cells including equine ECFCs, MCF7 cells, MDA-MB-231 cells, IMR90 hiPSCs, and 19-9-11 hiPSCs were detached from tissue culture flask, centrifuged, and resuspended in crosslinking precursor solution to the desired, application-specific cell density of 10-60 million cells mL^{-1}.

Cells encapsulation and hydrogel photocrosslinking were conducted in a biosafety cabinet to keep the process sterile. The device had two inlets and one outlet where cells and hydrogel precursor mixtures were flowed from the top inlet, and mineral oil was flowed from the bottom inlet by using syringe pumps. When the two streams meet at the junction, microspheres were formed due to emulsification and the cell-encapsulated microspheres were crosslinked by a 2.8W cm^{-2} full spectrum visible light (Prior Lumen 200). A mirror was placed behind the microfluidic device near the outlet to aid the crosslinking by reflecting the light that passed through the device. The microspheres

were washed down from the outlet with cell media by using a third syringe pump. The microspheres were then washed twice with media by centrifugation at 200 g for 3 min to remove the residual mineral oil and cultured in well plates at 37°C and 5% CO_2.

To prepare the microspheres shown in Figure 1G-J, the following experimental parameters were employed. The flow rates for mineral oil were 4, 10, 10, and 9 mL h^{-1}, respectively from G to J. The flow rates for hydrogel precursor solution were 0.8, 1, 0.5, and 1 mL h^{-1}, respectively. The flow rates for washing were 10 mL h^{-1} for all conditions. The junction diameters of microfluidic device were 240, 460, 520, and 460 µm, respectively. The outlet channel diameters of microfluidic device were 380, 960, 770, and 960 µm, respectively.

Microsphere geometry characterization: The uniformity of the microspheres was evaluated by measuring their maximum diameter and roundness on one and three days after cell encapsulation. Three batches of microspheres with at least 30 microspheres per batch were measured and the measurements were performed using ImageJ. Roundness measured in ImageJ is defined by **Equation 1**.

$$Roundness = \frac{Area}{\pi \times Major\ axis^2} \quad (1)$$

Uniformity was also analyzed by coefficient of variance (CV) which is defined by **Equation 2**.

$$Coefficient\ of\ variance = \frac{Standard\ deviation}{Mean} \quad (2)$$

Post-cell encapsulation cell viability assay: Cell viability after encapsulation was assessed by Live/Dead viability/cytotoxicity kit (Invitrogen). Cell-laden microspheres were incubated for 30 min with Calcein AM and Ethidium homodimer-1, and then Z-stack-images were obtained with fluorescence microscopy (Nikon Eclipse Ti). Three regions with same size (250 ×250 µm) were randomly selected from each microsphere using ImageJ, and both live and dead cells were counted through the optical slices along the z-axis for approximately 550 µm.

Scanning electron microscopy: The ultrastructural features of the microspheres and the cell-laden microspheres were visualized through scanning electron microscopy (SEM). Microspheres were washed with PBS, fixed with 4% glutaraldehyde (Electron Microscopy Sciences) for 1 hour and then fixed with 2% osmium tetroxide (Electron Microscopy Sciences) for 1 hour, all at room temperature. The fixed microspheres were frozen in liquid nitrogen for 2 minutes and then dried in a freeze dryer (Labconco). Dried samples were mounted on carbon taped-aluminum stubs, sputter-coated with gold (Pelco SC-6 sputter coater) and imaged using scanning electron microscope (JEOL JSM-7000F).

Microsphere stiffness: In order to measure the Young's modulus of the hydrogel microspheres, they were subjected to compression testing under physiological conditions using MicroSquisher (CellScale). Briefly, cell-laden hydrogel microspheres were loaded onto the MicroSquisher platform maintained at 37°C in PBS, preconditioned for compression testing and made to undergo cycles of compression and relaxation at a rate of 2.5 $\mu m\, s^{-1}$ for a minimum of 15% strain. The force-displacement data obtained from the stress were converted to stress-strain curves and the lower portion of the curve (5-15% strain) was used to estimate the Young's moduli of microspheres.

Immunocytochemistry: Encapsulated horse ECFCs were evaluated for the expression of cell proliferation maker Ki67 with indirect immunofluorescence assay (IFA). Microspheres cryosection containing ECFCs were fixed with 4% paraformaldehyde (PFA) solution and rinsed with PBS solution. ECFCs were then permeabilized with PBS-T containing 0.2% Triton X 100 (Sigma) in PBS for 30 minutes and blocked with 3% FBS at 4ºC overnight. The encapsulated cells were then incubated at room temperature for 2 hours with primary antibody solution which was rabbit anti-Ki67 (Abcam) at 1:100 dilution in 3% FBS solution. After incubation, cells were washed with PBS-T before applying secondary antibody. Alexa Fluor 680-conjugated goat anti-rabbit IgG diluted at 1:200 in 3% FBS solution was used as secondary antibody and incubated with cells at room temperature in dark for 2 hours. Cells were counterstained with DAPI, washed with PBS, mounted with ProLong Gold antifade reagent (Life technologies), and imaged with fluorescent microscopy.

Statistical analysis: All data were presented as mean ± standard deviation (SD). All statistical analysis was performed using Minitab 17 Statistical Software (Minitab Inc.). After verifying equal variances using F-test, Student's t-test was performed to evaluate statistical significance between two groups. After checking for normality of distribution, one-way analysis of variance (ANOVA) followed by the Tukey-Kramer honest significant difference (HSD) test was performed to evaluate statistical significance between multiple groups. Statistical significance was declared if $p<0.05$.

Supporting Information

Supporting Information is available from the Wiley Online Library or from the author.

Acknowledgements

Y.T. and W.J.S. contributed equally to this work. The authors wish to thank Dr. Anne Wooldridge from College of Veterinary Medicine for critical input on the development of the injectable cell delivery approach and Mr. Brennen Reece for providing the microfluidic platform illustration. The authors acknowledge funding support, in part, from the American Heart Association [AM HEART-14SDG18610002 (W.J.S., Y.T., and E.A.L.), the National Science Foundation Chemical, Bioengineering,

Environmental, and Transport Systems program [NSF-CBET-1150854 (E.A.L., P.K.)], Auburn University Research Initiative in Cancer (AURIC) (S.P.), and AL EPSCOR (P.K.).

Received: ((will be filled in by the editorial staff))
Revised: ((will be filled in by the editorial staff))
Published online: ((will be filled in by the editorial staff))

References

[1] M. P. Lutolf, J. A. Hubbell, *Nature Biotechnology* **2005**, 23, 47.

[2] V. L. Workman, L. B. Tezera, P. T. Elkington, S. N. Jayasinghe, *Advanced Functional Materials* **2014**, 24, 2648.

[3] R. Yao, R. J. Zhang, F. Lin, J. Luan, *Biofabrication* **2012**, 4.

[4] J. L. Horning, S. K. Sahoo, S. Vijayaraghavalu, S. Dimitrijevic, J. K. Vasir, T. K. Jain, A. K. Panda, V. Labhasetwar, *Molecular Pharmaceutics* **2008**, 5, 849.

[5] T. Shofuda, H. Fukusumi, D. Kanematsu, A. Yamamoto, M. Yamasaki, N. Arita, Y. Kanemura, *Neuroreport* **2013**, 24, 84.

[6] E. Dini, S. Alexandridou, C. Kiparissides, *Journal of Microencapsulation* **2003**, 20, 375.

[7] J. A. Tree, C. Richardson, A. R. Fooks, J. C. Clegg, D. Looby, *Vaccine* **2001**, 19, 3444.

[8] S. Tashiro, K. Tsumoto, E. Sano, *Journal of Biotechnology* **2012**, 160, 202.

[9] W. Y. Leong, D. A. Wang, *Trends in Biotechnology* **2015**, 33, 653.

[10] C. L. Franco, J. Price, J. L. West, *Acta Biomaterialia* **2011**, 7, 3267.

[11] S. Pradhan, J. M. Clary, D. Seliktar, E. A. Lipke, *Biomaterials* **2017**, 115, 141.

[12] Y. Y. Yang, T. S. Chung, N. P. Ng, *Biomaterials* **2001**, 22, 231.

[13] T. W. King, C. W. Patrick, *Journal of Biomedical Materials Research* **2000**, 51, 383.

[14] A. Khademhosseini, R. Langer, *Biomaterials* **2007**, 28, 5087.

[15] D. M. Headen, G. Aubry, H. Lu, A. J. Garcia, *Advanced Materials* **2014**, 26, 3003.

[16] D. Velasco, E. Tumarkin, E. Kumacheva, *Small* **2012**, 8, 1633.

[17] W. J. Seeto, Y. Tian, R. L. Winter, F. J. Caldwell, A. A. Wooldridge, E. A. Lipke, *Tissue Engineering Part C-Methods* **2017**, 23, 815.

[18] Z. L. Jiang, B. Z. Xia, R. McBride, J. Oakey, *Journal of Materials Chemistry B* **2017**, 5, 173.

[19] X. Zhao, S. Liu, L. Yildirimer, H. Zhao, R. H. Ding, H. N. Wang, W. G. Cui, D. Weitz, *Advanced Functional Materials* **2016**, 26, 2809.

[20] D. Baah, T. Floyd-Smith, *Microfluidics and Nanofluidics* **2014**, 17, 431.

[21] J. H. Xu, S. W. Li, J. Tan, G. S. Luo, *Microfluidics and Nanofluidics* **2008**, 5, 711.

[22] H. Kim, D. W. Luo, D. Link, D. A. Weitz, M. Marquez, Z. D. Cheng, *Applied Physics Letters* **2007**, 91.

[23] S. L. Anna, N. Bontoux, H. A. Stone, *Applied Physics Letters* **2003**, 82, 364.

[24] S. Wang, A. Bruning, O. Jeon, F. Long, E. Alsberg, C. K. Choi, *Biomicrofluidics* **2018**, 12.

[25] J. Clausell-Tormos, D. Lieber, J. C. Baret, A. El-Harrak, O. J. Miller, L. Frenz, J. Blouwolff, K. J. Humphry, S. Koster, H. Duan, C. Holtze, D. A. Weitz, A. D. Griffiths, C. A. Merten, *Chemistry & Biology* **2008**, 15, 427.

[26] K. T. Nguyen, J. L. West, *Biomaterials* **2002**, 23, 4307.

[27] D. Seliktar, *Science* **2012**, 336, 1124.

[28] P. Kerscher, J. A. Kaczmarek, S. E. Head, M. E. Ellis, W. J. Seeto, J. Kim, S. Bhattacharya, V. Suppiramaniam, E. A. Lipke, *Acs Biomaterials Science & Engineering* **2017**, 3, 1499.

[29] S. R. Shin, C. Zihlmann, M. Akbari, P. Assawes, L. Cheung, K. Z. Zhang, V. Manoharan, Y. S. Zhang, M. Yuksekkaya, K. T. Wan, M. Nikkhah, M. R. Dokmeci, X. W. Tang, A. Khademhosseini, *Small* **2016**, 12, 3677.

[30] C. Sonnet, C. L. Simpson, R. M. Olabisi, K. Sullivan, Z. Lazard, Z. Gugala, J. F. Peroni, J. M. Weh, A. R. Davis, J. L. West, E. A. Olmsted-Davis, *Journal of Orthopaedic Research* **2013**, 31, 1597.

[31] G. Odian, *Principles of polymerization*, John Wiley & Sons, **2004**.

[32] N. Annabi, J. W. Nichol, X. Zhong, C. D. Ji, S. Koshy, A. Khademhosseini, F. Dehghani, *Tissue Engineering Part B-Reviews* **2010**, 16, 371.

[33] J. H. Xu, S. W. Li, J. Tan, Y. J. Wang, G. S. Luo, *Aiche Journal* **2006**, 52, 3005.

[34] M. M. Dupin, I. Halliday, C. M. Care, *Physical Review E* **2006**, 73.

[35] J. C. McDonald, D. C. Duffy, J. R. Anderson, D. T. Chiu, H. K. Wu, O. J. A. Schueller, G. M. Whitesides, *Electrophoresis* **2000**, 21, 27.

[36] E. Brouzes, M. Medkova, N. Savenelli, D. Marran, M. Twardowski, J. B. Hutchison, J. M. Rothberg, D. R. Link, N. Perrimon, M. L. Samuels, *Proceedings of the National Academy of Sciences of the United States of America* **2009**, 106, 14195.

[37] C. Kropp, D. Massai, R. Zweigerdt, *Process Biochemistry* **2017**, 59, 244.

[38] V. Mironov, R. P. Visconti, V. Kasyanov, G. Forgacs, C. J. Drake, R. R. Markwald, *Biomaterials* **2009**, 30, 2164.

[39] C. H. Choi, J. H. Jung, Y. W. Rhee, D. P. Kim, S. E. Shim, C. S. Lee, *Biomedical Microdevices* **2007**, 9, 855.

[40] S. Koster, F. E. Angile, H. Duan, J. J. Agresti, A. Wintner, C. Schmitz, A. C. Rowat, C. A. Merten, D. Pisignano, A. D. Griffiths, D. A. Weitz, *Lab on a Chip* **2008**, 8, 1110.

[41] A. Kumachev, J. Greener, E. Tumarkin, E. Eiser, P. W. Zandstra, E. Kumacheva, *Biomaterials* **2011**, 32, 1477.

[42] R. Zhang, B. A. Le, W. Xu, K. Guo, X. M. Sun, H. Y. Su, L. Huang, J. Y. Huang, T. Shen, T. Liao, Y. Y. Liang, J. X. J. Zhang, H. J. Dai, K. Qian, *Small Methods* **2019**, 3.

[43] S. Jadhav, C. D. Eggleton, K. Konstantopoulos, *Biophysical Journal* **2005**, 88, 96.

[44] R. Zhang, C. Rejeeth, W. Xu, C. Y. Zhu, X. Y. Liu, J. J. Wan, M. W. Jiang, K. Qian, *Analytical Chemistry* **2019**, 91, 7078.

[45] L. Hidalgo San Jose, P. Stephens, B. Song, D. Barrow, *Tissue Engineering: Part C* **2018**, 24.

[46] W. H. Tan, S. Takeuchi, *Advanced Materials* **2007**, 19, 2696.

[47] L. Capretto, S. Mazzitelli, G. Luca, C. Nastruzzi, *Acta Biomaterialia* **2010**, 6, 429.

[48] G. Orive, M. De Castro, S. Ponce, R. M. Hernandez, A. R. Gascon, M. Bosch, J. Alberch, J. L. Pedraz, *Molecular Therapy* **2005**, 12, 283.

[49] S. J. Bidarra, C. C. Barrias, M. A. Barbosa, R. Soares, P. L. Granja, *Biomacromolecules* **2010**, 11, 1956.

[50] S. Sakai, S. Ito, H. Inagaki, K. Hirose, T. Matsuyama, M. Taya, K. Kawakami, *Biomicrofluidics* **2011**, 5.

[51] M. M. Salter, W. J. Seeto, B. B. DeWitt, S. A. Hashimi, D. D. Schwartz, E. A. Lipke, A. A. Wooldridge, *American Journal of Veterinary Research* **2015**, 76, 174.

[52] S. A. DeLong, A. S. Gobin, J. L. West, *Journal of Controlled Release* **2005**, 109, 139.

[53] L. Almany, D. Seliktar, *Biomaterials* **2005**, 26, 2467.

[54] J. W. Nichol, S. T. Koshy, H. Bae, C. M. Hwang, S. Yamanlar, A. Khademhosseini, *Biomaterials* **2010**, 31, 5536.

[55] A. I. Van Den Bulcke, B. Bogdanov, N. De Rooze, E. H. Schacht, M. Cornelissen, H. Berghmans, *Biomacromolecules* **2000**, 1, 31.

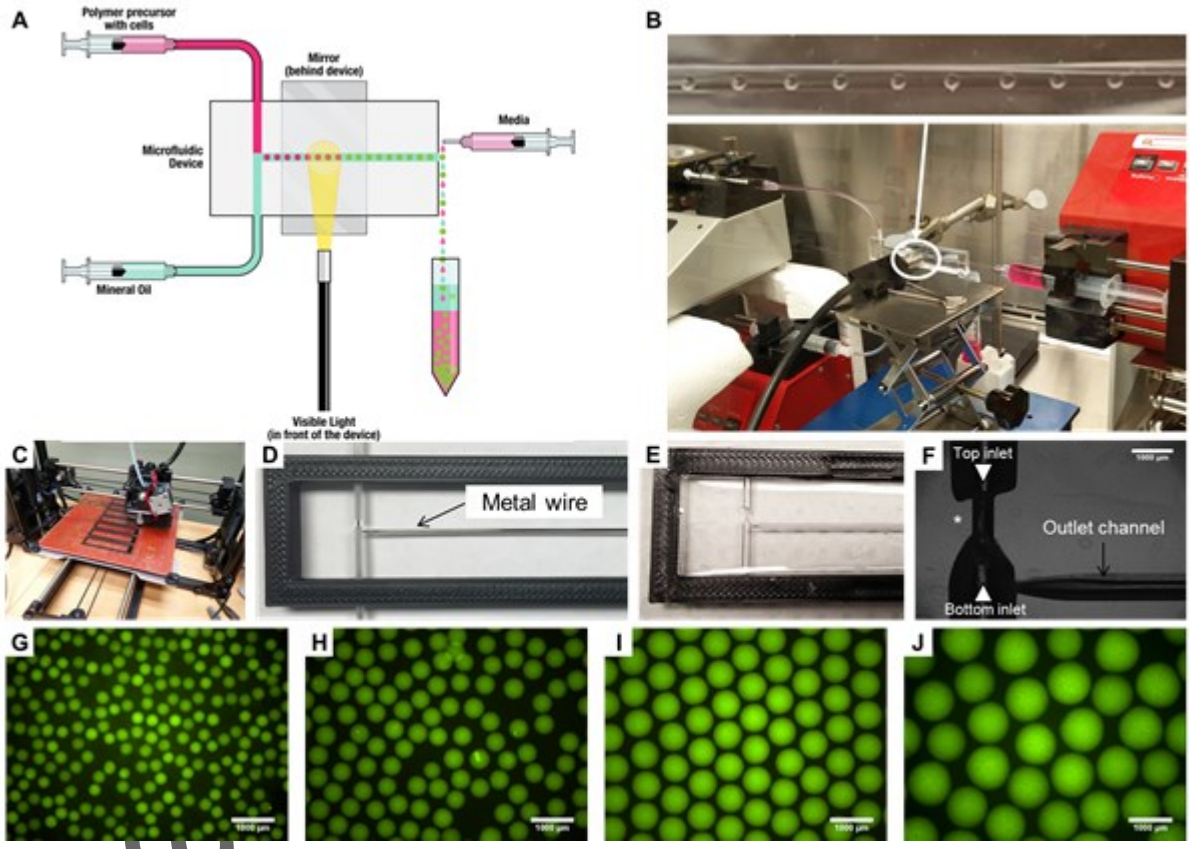

Figure 1. Microfluidic encapsulation platform using a novel custom design and device molding technique enables production of uniform hydrogel microspheres with a wide range of diameters. A) Schematic of the microfluidic encapsulation platform. B) Setup of the microfluidic encapsulation platform in a biosafety cabinet. Microsphere production video is shown in **Video S1** (Supporting Information). C) 3D printing of the jig. The jig helps with consistent, low-cost, and scalable production of microfluidic devices. Design of the jig is shown in Figure S1 (Supporting Information). D) The printed reusable jig holds the assembly of the channels together. The T-junction and the channels are molded with Teflon tubes and metal wires, enabling quick fabrication of prototypes for ready testing and design iteration, which is beneficial for understanding the fluid dynamics during microsphere production. E) PDMS microfluidic device after curing and channel mold removal. F) T-junction of the microfluidic device with precursor inlet on top and mineral oil inlet from bottom. The restriction segment for stabilization of the precursor/oil interface is indicated by an asterisk. (G-J) Hydrogel microspheres with a wide range of diameters (from 300 µm to 1100 µm) can be produced using the microfluidic encapsulation platform. The diameters of microspheres

shown in the figures are 312 ± 13, 473 ± 15, 723 ± 7, and 1008 ± 47 µm respectively (n>20 microspheres per condition, experimental parameters are included in the Experimental Section). The hydrogel microspheres are shown in fluorescent green due to the Eosin Y used during photocrosslinking.

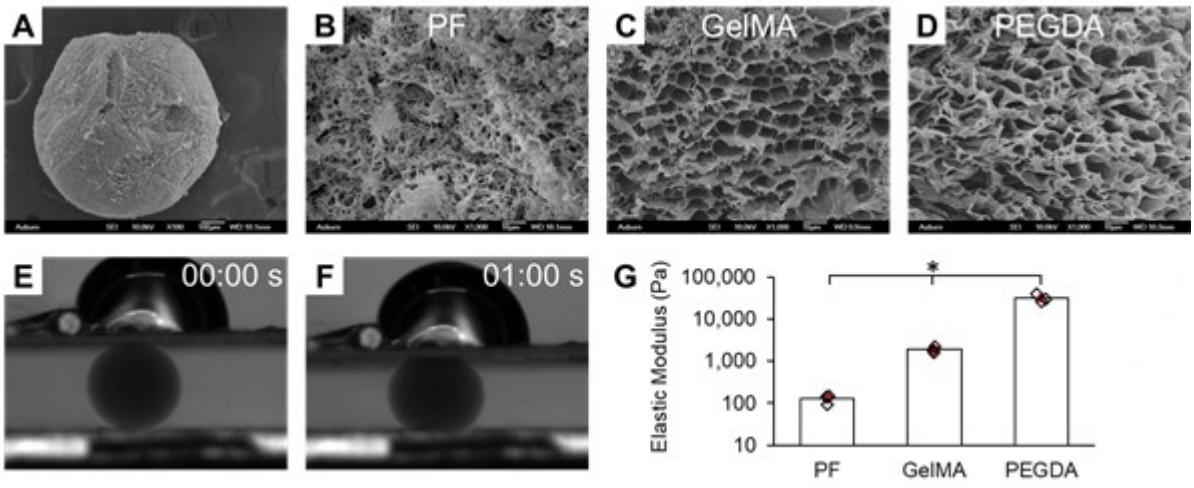

Figure 2. Microspheres were able to be formed using a range of photocrosslinkable hydrogel materials. Porous structure of the hydrogel scaffolds shown by SEM of (A) GelMA microspheres (100x), (B) PF microspheres (1000x), (C) GelMA microspheres (1000x), and (D) PEGDA microspheres (1000x). (E-F) Compression testing was used to assess elastic moduli of the microspheres. Compression testing video is shown in **Video S2** (Supporting Information). G) Elastic moduli of PF, GelMA, and PEGDA were found to be 127.3±24.4 Pa, 1894±257 Pa, and 31,800±5,280 Pa respectively (n=3 separate measurements for each material). Elastic moduli were found to be significantly different between different materials (*p<0.05).

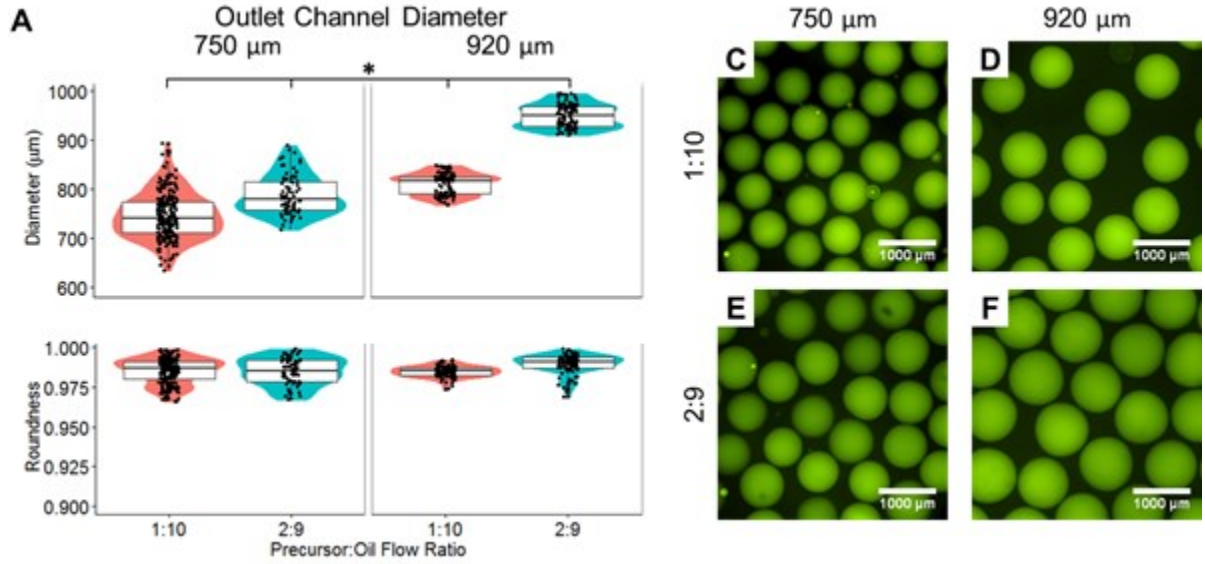

Figure 3. Microfluidic device provides tight control over microsphere diameter. A) Hydrogel precursor to oil flow rate ratio and outlet channel diameter are critical in determining microsphere diameter. By changing the flow ratio or the outlet channel diameter, the size of microspheres can be adjusted. Diameters were found to be significantly different between all pairs (*$p<0.05$, $n>78$ microspheres per condition). B) Roundness (above 0.95) was maintained under all conditions. (C-F) The change of microspheres in size under different experimental conditions shown by fluorescent images.

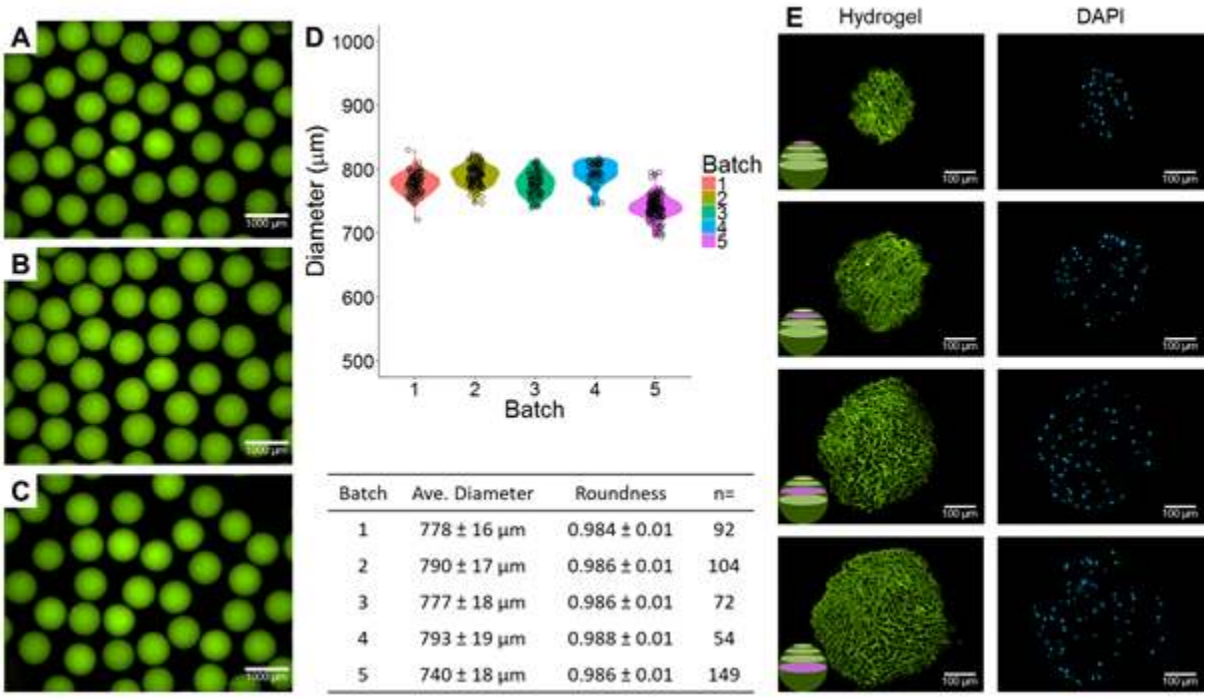

Batch	Ave. Diameter	Roundness	n=
1	778 ± 16 µm	0.984 ± 0.01	92
2	790 ± 17 µm	0.986 ± 0.01	104
3	777 ± 18 µm	0.986 ± 0.01	72
4	793 ± 19 µm	0.988 ± 0.01	54
5	740 ± 18 µm	0.986 ± 0.01	149

Figure 4. Microfluidic encapsulation platform enables high uniformity of microspheres both between and within batches. (A-C) PF microspheres with encapsulated horse ECFCs from 3 separate batches. D) Tight control of microsphere size and shape was achieved by the microfluidic encapsulation platform within and between batches (n>54 microspheres per batch). Microsphere average diameter ranged from 740 µm to 793 µm between batches with low variance within each batch. The roundness was above 0.980 with the standard deviation of 0.01 for all batches. E) Cell distribution throughout the microsphere post-encapsulation shown by cryosections of ECFC microspheres. Hydrogel structure visualized in green (Eosin Y), nuclei in blue (DAPI). Inset schematic shows slice location based on measured diameter (Pink).

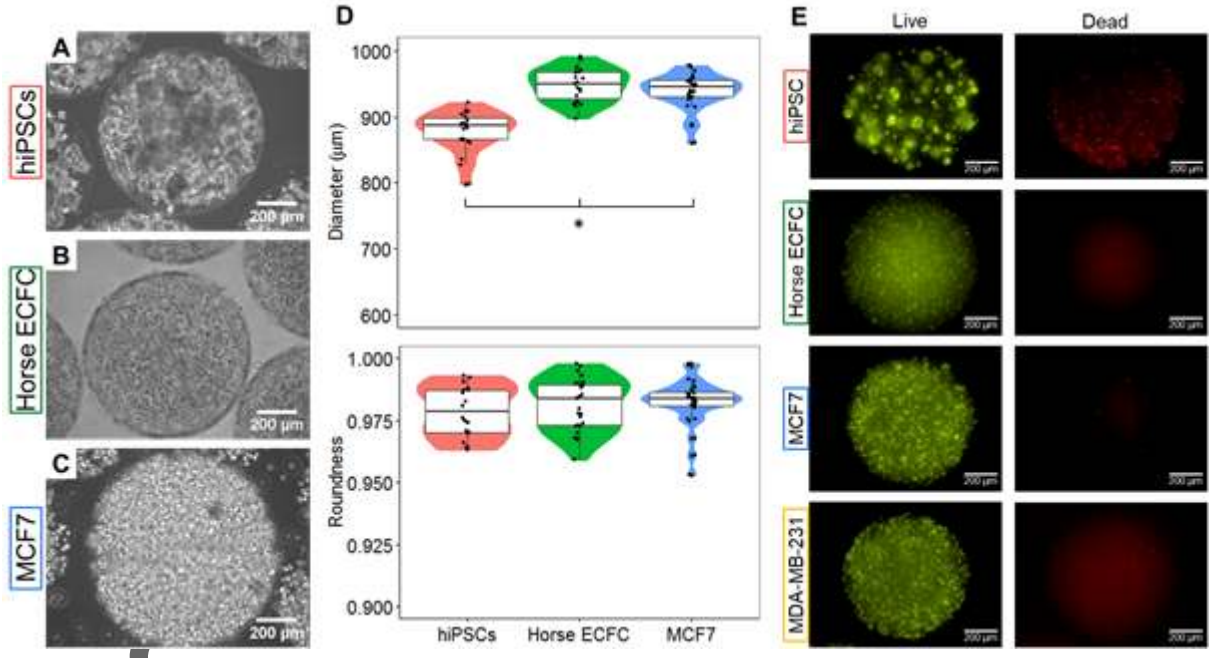

Figure 5. Uniform microspheres with high cell densities can be fabricated for a range of cell types using the microfluidic encapsulation platform. Phase contrast images of (A) hiPSCs (25 million cells mL^{-1}) (B) horse ECFCs (10 million cells mL^{-1}), and (C) MCF7 breast cancer cells (20 million cells mL^{-1}) encapsulated in PF microspheres. Encapsulation of single cells (ECFCs, MCF7 cells) and cell clusters (hiPSCs) was readily achievable; **Figure S2**A-B (Supporting Information) shows batch-to-batch comparisons for each cell type. D) Diameters of hiPSCs, horse ECFC, and MCF7 microspheres are 878 ± 29 µm, 957 ± 31 µm, and 939 ± 26 µm (n>20 microspheres for each cell type). Microsphere diameter was found to differ significantly between cell types (*$p<0.05$), possibly as a result of differences in cell size, cell encapsulation density, and pre-encapsulation cell dissociation method (clusters versus single cells). High degree of roundness (above 0.95) was maintained for all cell types. E) All tested cell types maintained high viability post encapsulation within PF microspheres (Live Green: Calcein AM, Dead Red: Ethidium homodimer).

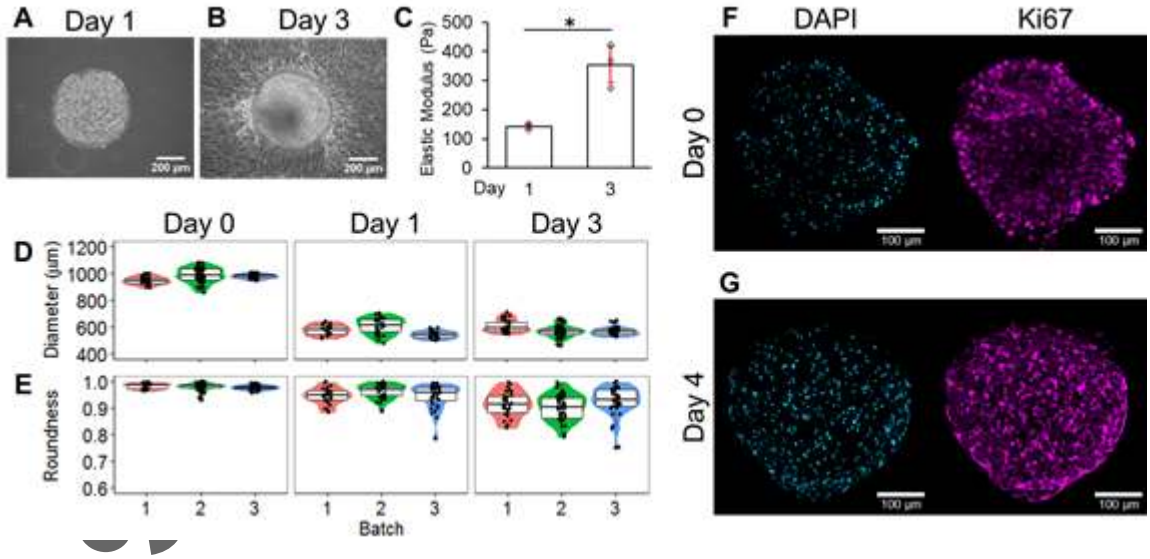

Figure 6. ECFCs maintained their highly proliferative phenotype post-encapsulation in PF microspheres. (A-B) Outgrowth of ECFCs from microspheres indicating high proliferative capability was maintained post encapsulation. C) The elastic modulus of microspheres with horse ECFCs have significantly increased from 142 ± 10 Pa on day 1 to 354 ± 62 Pa on day 3 (*$p<0.05$, $n>4$ microspheres per condition). Changes in elastic modulus were also measured for microspheres with cancer cells and hiPSCs (results shown in Figure S2C, Supporting Information). (D-E) ECFCs remodeled the microsphere size and shape during culture. Similar cellular activities were observed over time on multiple batches of ECFC-laden microspheres cultured over a month (shown in Figure S3, Supporting Information). (F-G) Encapsulated ECFCs remained proliferative within the microspheres as shown by the expression of cell proliferation marker Ki67 (Blue: DAPI, Magenta: Ki67).

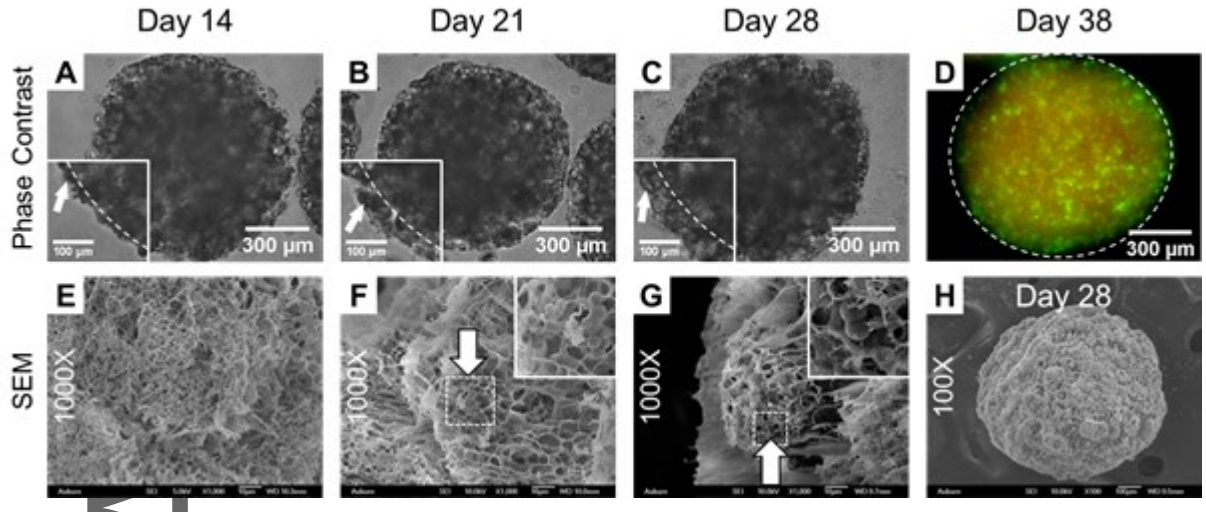

Figure 7. Encapsulated cells were able to be cultured for an extended time post-encapsulation. (A-C) Increasing colony outgrowth of cancer cells from MCF7 microspheres,

indicating proliferation of cells during long-term culture. Initial microsphere boundaries are indicated by a dashed line. D) Encapsulated MDA-MB-231 cells maintained high viability for a long-term. Viability assay was conducted on day 38 post-encapsulation (Live Green: Calcein AM, Dead Red: Ethidium homodimer). Separate live, dead, and nuclei images are shown in **Figure S4** (Supporting Information). (E-H) SEM images of MCF7 microspheres with magnification of 1000x and 100x. Cancer cell colonies are indicated by arrows.

Figure 8. Summary of the advantages of the established microfluidic encapsulation platform.

Table 1. Cells encapsulated with high densities.

Cell Type	Initial Cell Concentration Used [x 10^6 cells mL^{-1}]	Diameter (µm) (CV)	Roundness (CV)	Potential Applications
ECFC	10	957 ± 31 (0.03)	0.98 ± 0.01 (0.01)	Cell delivery
hiPSC	25	878 ± 29	0.98 ±	Stem cell

		0.01 (0.03)	0.01 (0.01)	differentiation
Breast cancer (MCF7)	20	939 ± 26 (0.03)	0.98 ± 0.01 (0.01)	Cancer tissue model
Breast cancer (MCF7)	60	979 ± 13 (0.01)	0.98 ± 0.01 (0.01)	Cancer tissue model

Table 2. Comparison of established microfluidic platform attributes to existing cell-laden microsphere production systems.

Production method (References)	Microfluidic (This manuscript)	Microfluidic [15,45,46,47]	Nozzle-based droplet generator [48,49]	Microfluidic [41,50]	Microfluidic [18,19]
Crosslinking method	Photo	Chemical	Chemical	Thermal	Photo
Rapid crosslinking	**++**	-	-	-	**+**
Junction design	Modified T-junction with vertical orientation	T-junction/ Flow focusing	n/a	T-junction/ Flow focusing	T-junction/ Flow focusing
Rapid/simple device fabrication	**+** (Molding)	- (Photolithography)	-	- (Photolithography)	- (Photolithography)

with low cost					
Wide range of sizes	++	-	+	-	-
Support multiple materials	+	-	-	-	+
High cell density ($>10^6$ mL^{-1})	++	-	+	+	-
High production rate (>1 mL h^{-1})	+	+	++	+	-
High uniformity	+	+	+	+	+

Title: Rapid production of cell-laden microspheres using a flexible microfluidic encapsulation platform

Authors: W. J. Seeto, Y. Tian, S. Pradhan, P. Kerscher, E. A. Lipke*

Table of contents summary:

A novel microfluidic encapsulation platform is designed and used for rapid production of highly uniform cell-laden hydrogel microspheres with high cell densities and a wide range of sizes, which cannot be achieved using traditional microfluidic chips. With all the features, the resulting microspheres advance the ability to use tissue microspheres for downstream applications including regenerative medicine.

Keywords: bioreactor-based cell manufacturing, injectable cell therapy, high throughput drug screening, 3D bioprinting

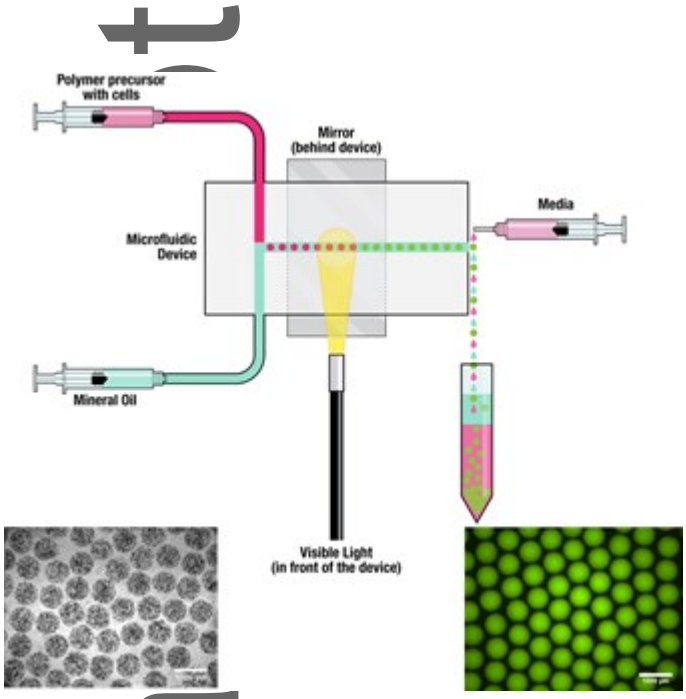

Table of Contents figure (also provide as TIFF):